The Crystal Structure of Mitochondrial Cytochrome *bc1* in Complex with Famoxadone: The Role of Aromatic−Aromatic Interaction in Inhibition[†,‡]

Xiugong Gao,[§] Xiaolin Wen,[||] ChangAn Yu,[||] Lothar Esser,[§] Scott Tsao,[||] Byron Quinn,[||] Li Zhang,[||] Linda Yu,[||] and Di Xia*[,§]

Laboratory of Cell Biology, Center for Cancer Research, National Cancer Institute, National Institutes of Health, Bethesda, Maryland 20892, and Department of Biochemistry and Molecular Biology, Oklahoma State University, Stillwater Oklahoma 74078

Received June 6, 2002; Revised Manuscript Received July 17, 2002

ABSTRACT: Ubiquinol cytochrome *c* oxido-reductase (EC. 1.10.2.2, *bc1*) is an integral membrane protein complex essential to cellular respiration. Structures of the 11-subunit mitochondrial *bc1* complex were determined with and without the fungicide famoxadone. Specific inhibition by famoxadone is achieved through a coordinated optimization of aromatic−aromatic interactions where conformational rearrangements in famoxadone and in residues lining the inhibitor-binding pocket produce a network of aromatic−aromatic interactions that mimic the crystal lattice of benzene. The profound aromatic−aromatic interactions as supported by prior mutagenesis provide a structural basis for specific protein−ligand interaction in a hydrophobic environment. Dramatic conformational changes, both in cyt. *b* and ISP subunits in the inhibitor-protein complex, confer experimental evidence for a functional role of cytochrome *b* in the induced conformational arrest of ISP and allow the identification of a possible intrasubunit signal transduction pathway that controls the movement of ISP. These results support an inhibitory mechanism that is consistent with the requirement for ISP movement in the electron transfer of this complex.

Cellular respiration requires coupling of a series of oxidation and reduction steps to proton translocation across biological membranes to create a proton-motive force for ATP synthesis. The cytochrome *bc1* complex is an essential component in the respiratory chain; it catalyzes electron transfer from quinol to cyt. *c* and concomitantly translocates protons across membranes (*1*−*4*). *Bc1* is a dimeric multi-subunit integral membrane protein complex (*5*−*7*); subunit composition varies from three subunits in the prokaryote *Paracoccus denitrificans* to 11 subunits in eukaryotes as in bovine mitochondria. Essential subunits for ET in *bc1* include one cyt. *b* containing two *b*-type hemes (b_L and b_H), one cyt. *c1* containing a *c*-type heme, and one ISP containing a 2Fe−2S cluster. The proton-motive Q cycle hypothesis (*8*−*10*) postulates two quinone reaction sites in *bc1*: namely, the Q_o site for quinol oxidation and the Q_i site for quinone reduction. It further assumes a bifurcated ET at the Q_o site where two electrons from a quinol molecule diverge in two directions: one goes through the high-potential ISP to cyt. *c1*, ending up in substrate cyt. *c*; the other through the low-potential b_L heme and the high-potential b_H heme sequentially, reaching the acceptor quinone at the Q_i site.

Structural information for the *bc1* complex was obtained primarily from crystallographic studies of eukaryotic mitochondrial *bc1* (*6*, *11*−*15*). For the bovine complex, the dimer has a molecular mass of near 500 kDa and consists of three regions: a TM region containing 26 membrane-spanning helices, a very large matrix region, and an IMS region. The three functionally important subunits are either integrated to or anchored in the membrane; the cyt. *b* monomer has eight TM helices, whereas cyt. *c1* and ISP each contain one TM helix with large portions of *c1* and ISP in the IMS.

Crystallographic evidence (*6*, *11*−*13*), augmented by genetic studies (*16*−*20*), suggests that bifurcated ET at the Q_o site may be achieved through intramolecular motion of the subunit ISP that serves as an electron carrier shuttling between the Q_o site and cyt. *c1*. Respiratory inhibitors specifically targeted at *bc1* are grouped into two classes: class I inhibitors such as myxothiazol and stigmatellin block the ET path at the Q_o site and those in class II like antimycin A block at the Q_i site. Class I inhibitors are further divided into three subclasses based on their effects on spectroscopic properties of the b_L heme and the ISP (*21*). Class Ia (e.g. myxothiazol, MOAS) affects only b_L heme spectra; class Ib (e.g., UHDBT) causes changes in EPR spectra of ISP, and

[†] This work was supported in part by an NIH grant to CAY (GM-30721).

[‡] The atomic coordinates have been deposited for release with publication in the Protein Data Bank with accessions numbers 1LOL and 1LON.

* Corresponding author. Address: Laboratory of Cell Biology, CCR, NCI, NIH, 37 Convent Dr. Building 37, Room 1B22, Bethesda, MD 20892. Tel.: 301-435-6315. Fax: 301-435-8188. E-mail: dixia@helix.nih.gov.

[§] National Cancer Institute.

[||] Oklahoma State University.

[1] Abbreviations: *bc1*, ubiquinol cytochrome *c* oxidoreductase; cyt. *b*, cytochrome *b* subunit; cyt. *c1*, cytochrome *c1* subunit; ISP, iron sulfur protein subunit; ET, electron transfer; Q_o, quinol oxidation; Q_i, quinone reduction; QH_2, ubiquinol; b_L, low-potential heme; b_H, high-potential heme; 2Fe−2S, two iron two sulfur cluster; Ar−Ar, aromatic−aromatic interaction; TM, trans-membrane helix; IMS, intermembrane space; MOAS, methoxy acrylate stilbene; UHDBT, 5-undecyl-6-hydroxy-4,7-dioxobenzothiazol; EPR, electron paramagnetic resonance; rmsd, root-mean-square deviation.

10.1021/bi026252p CCC: $22.00
Published on Web 09/05/2002

Table 1: Statistics of Crystallographic Data Collection and Structure Refinement

	native[a]	famoxadone[a]
Crystallographic Diffraction Data Statistics		
resolution (Å)	80−2.6	80−2.4
unit cell (Å)[b]	*a* = *b* = *153.8*, *c* = *596.7*	*a* = *b* = *154.1*, *c* = *591.8*
R_{merge}[c]	0.061	0.057
(outer shell)	(0.520)	(0.339)
completeness	95.2	95.2
(outer shell)	(96.7)	(96.7)
ano. R_{merge}	0.056	0.054
(outer shell)	(0.458)	(0.309)
ano. completeness	90.0	83.4
(outer shell)	(89.8)	(72.9)
no. of unique reflections	104,476	123,427
no. of free reflections	2,122	2,461
Crystallographic Refinement Statistics		
R_{work}	0.261	0.259
R_{free}	0.297	0.306
no. of atoms	16,800	17,381
no. of residues	2,113	2,135
no. of cofactors	4	4
no. of solvent molecules	447	432
rmsd[d] bond distance (Å)	0.02	0.03
rmsd[d] bond angles (°)	1.9	2.1

[a] Statistics for both data sets are computed at -1σ cutoff, and both data sets were collected at 1.0 Å wavelength. [b] Space group symmetry for both native and the famoxadone bound *bc1* crystal are $I4_122$. [c] R_{merge} is defined as $\Sigma|I_{\mathbf{h},i} - \langle I_{\mathbf{h}}\rangle|/\Sigma I_{\mathbf{h},i}$ where $I_{\mathbf{h},i}$ is the intensity for *i*th observation of a reflection with Miller index **h** and $\langle I_{\mathbf{h}}\rangle$ is the mean intensity for all measured $I_{\mathbf{h}}$s and Freidel pairs. [d] rmsd is the root-mean-square deviation of bond distance or bond angle in *bc1* crystal with respect to those of standard parameters.

class Ic (e.g., stigmatellin) confers changes in both. Furthermore, classe Ib and Ic inhibitors often lead to elevated redox potential of ISP. Multiple orientations and positions of ISP soluble domain have been observed in different crystal forms (*6*, *11*, *12*), and at least two conformational states in the soluble domain of ISP in response to binding of class I inhibitors were reported: a fixed and a loose state (*13*, *22*). In the fixed state, ISP binds tightly to cyt. *b* with the 2Fe−2S cluster very close to the putative Q_o site; in the loose state, ISP does not prefer any particular position between cyt. *c1* and cyt. *b*. Binding of class Ib and Ic inhibitors favors ISP in the fixed state, whereas binding of class Ia inhibitors promotes the loose state. The mechanism that triggers ISP movement remains unknown.

Aromatic molecules such as benzene tend to associate with each other in a unique edge-to-face arrangement that was termed Ar−Ar interaction originating from local dipole−dipole interactions between partially positively charged hydrogen atoms and negatively charged aromatic rings. The Ar−Ar interaction has been used to describe benzene in the crystalline state (*23*) and is responsible for the high melting point of benzene (+5.5 °C). In comparison, water, with its extensive network of H-bonds, stays liquid above 0 °C, and cyclohexane, having C−H dipoles but lacking the aromatic ring system, freezes at −103.5 °C (*24*). Survey of protein structures revealed ample examples of single pair Ar−Ar interactions thought to stabilize folded proteins (*25*). Mutational studies of ribonuclease demonstrated that a single pair of Ar−Ar interaction could provide −1.3 kcal/mol of free energy (*26*). Unlike hydrophobic interactions, the Ar−Ar interaction is in principle specific and effective within short-range, favors a hydrophobic environment, and could potentially be exploited to optimize ligand-protein interaction. Famoxadone [5-methyl-5-(4-phenoxy-phenyl)-3-phenylamino-2,4 oxazolidinedione] is a specific Q_o site *bc1* inhibitor with three aromatic rings developed for control of fungal disease in crops (*27*). The inhibitor has one chiral center; only the S-enantiomer is active for inhibition. Binding of this inhibitor to *bc1* causes the b_L heme spectrum red shift that resembles the effect of myxothiazol binding (*27*) but does not produce an observable change to the EPR spectrum of ISP. Although the molecular modeling and crystal structure of famoxadone demonstrated that an extended conformation for the molecule was energetically favorable (*28*), the conformation in complex with *bc1* was not investigated.

To understand the mechanism of ET in *bc1*, especially the mechanics that controls the ISP movement, and the mode of inhibition by famoxadone, we investigated the structure of bovine *bc1* in complex with the inhibitor.

EXPERIMENTAL PROCEDURES

Protein Purification and Crystallization. The purified *bc1* complex from bovine heart mitochondria was prepared, starting from highly purified succinate-cyt. *c* reductase, as previously reported (*29*). The *bc1* particles were solublilized by deoxycholate, and contaminants were removed by a 15-step ammonium acetate fractionation. Pure *bc1* complex in oxidized form was recovered from the precipitates formed between 18.5% and 33.5% ammonium acetate saturation. The final product was dissolved in 50 mM Tris−HCl buffer, pH 7.8, containing 0.66 M sucrose to a protein concentration of 30 mg/mL, and frozen at −80 °C until use. The concentrations of cyt. *b* and *c1* were determined spectroscopically, using millimolar extinction coefficients of 28.5 and 17.5 for cyt. *b* and *c1*, respectively. The homogeneity in redox state of *bc1*was confirmed spectrophotometrically.

Purified *bc1* complexes were adjusted to a final concentration of 20 mg/mL in a solution containing 50 mM MOPS buffer at pH 7.2, 20 mM ammonium acetate, 20% (w/v) glycerol, and either 0.1% of decanoyl-*N*-methylglucamide or 0.1% of diheptanoyl phosphatidylcholine or 0.16% of

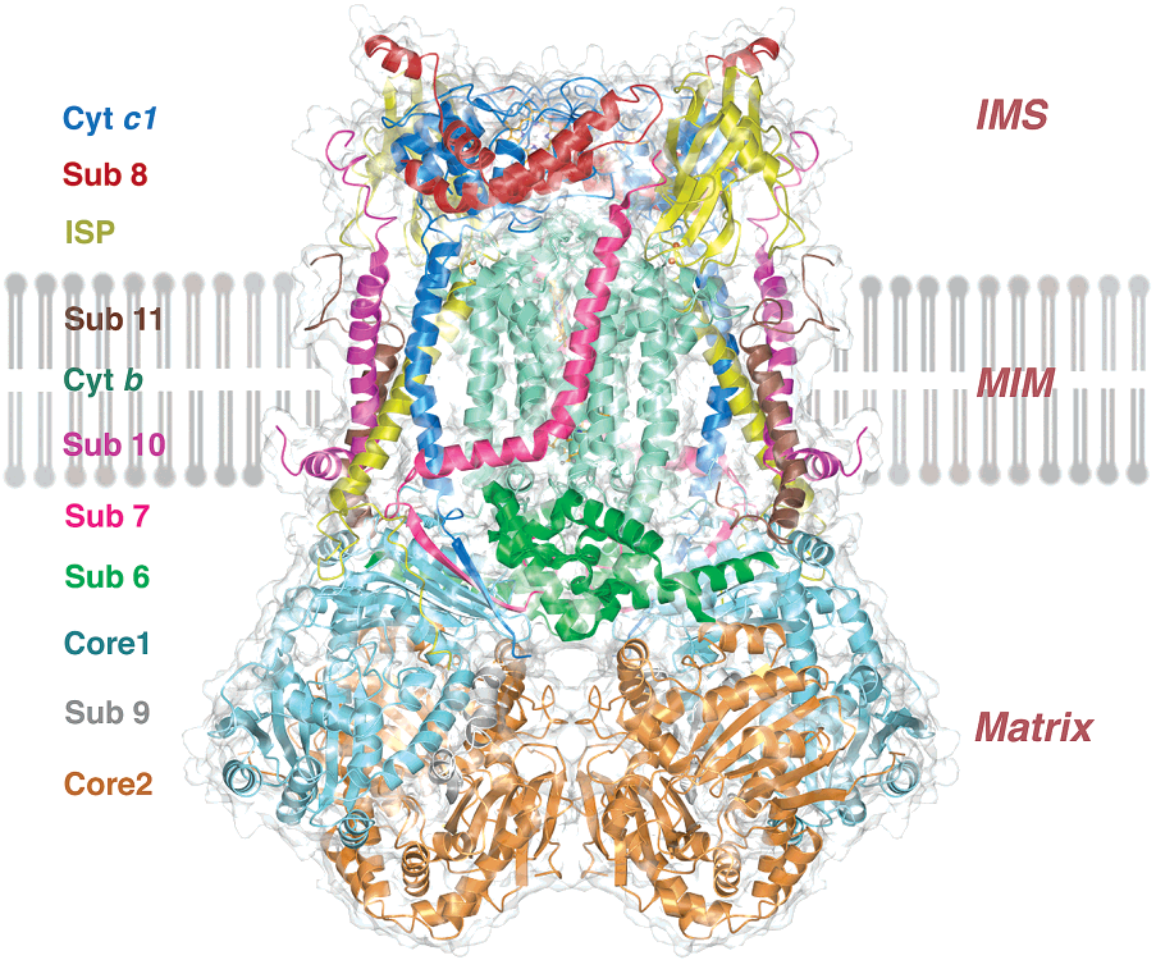

FIGURE 1: Ribbon diagram of the dimeric mitochondrial cyt. *bc1* complex. The ribbon model is enclosed in a semitransparent molecular surface produced with the GRASP program (*41*). Colors identifying the subunits are given at the left margin. Position of the membrane bilayer is delineated based on lipid molecules identified in the structure. The molecule is oriented with the intermembrane space (IMS) side at top, the matrix side at the bottom, and the mitochondrial inner membrane (MIM) in between. The ribbon diagram was produced with the programs Molscript (*42*), Bobscript (*43*) and POVRAY (www.povray.org) interfaced with Gl-render (Esser, unpublished work).

sucrose monocaprate. This solution was set up for crystallization as described in previous publications (*6*, *30*). Native crystals were grown in either sitting or hanging drops and appeared in 3−4 weeks. The famoxadone bound *bc1* crystals were grown under conditions similar to those of native crystals except that a 5-fold molar excess of famoxadone was added to the protein solution prior to crystallization. Both native and famoxadone bound *bc1* crystal had a rectangular shape ranging in sizes from 0.4 to 0.7 mm and were cryoprotected at a glycerol concentration of 30−40%. These crystals invariably possess the same symmetry of space group $I4_122$ and similar unit cell dimensions (Table 1).

X-Ray Diffraction Data Collection and Reduction. Crystals of bovine mitochondrial *bc1* complex with and without bound inhibitor were stable when cryo-cooled to 100 K at synchrotron radiation sources, permitting several hours of data collection. Data sets reported in this study were collected at the beamline BioCARS-CAT of Advanced Photon Source (APS), Argonne National Lab (ANL), and a wavelength of 1.0 Å was used. The native and inhibitor-bound crystals diffracted X-rays anisotropically up to 2.6 and 2.4 Å resolution, respectively (Table 1). Raw diffraction frames were processed with the program DENZO, and integrated intensities from each diffraction image of the same crystal were merged and scaled with the program SCALEPACK. Both programs are part of the HKL program package (*31*). Bijvoet pairs were kept separate in all data processing procedures. The current native data set with reflections extending to an effective resolution of 2.6 Å is superior to the 2.9 Å data set previously reported (*6*). For the complex, reflections beyond 2.4 Å resolution fail to follow the Wilson statistics (*32*) and were not used in the refinement.

Structure Refinement, Modeling, and Analysis. Diffraction data sets for both native and complex crystals were phased separately with coordinates of the 11-subunit *bc1* model (*6*). The program REFMAC (*33*) was used for initial rigid-body refinement followed by iterative maximum-likehood and TLS (translation, libration, and screw tensor) refinement. Between REFMAC runs, σA (*34*) weighted $2F_o-F_c$ and F_o-F_c maps were calculated with the FFT program (*35*) and used to identify and build bound ligand and solvent molecules with the program O (*36*), which were included in subsequent refinement cycles. The initial coordinates for famoxadone were obtained from the published crystal model (*28*) and subsequently refined against the diffraction data of a complex crystal. The statistics for the refinement and model quality of both the native and the complex *bc1* crystals are also given in Table 1. Structure alignment between the native and the inhibitor complex, as well as between Q_o pocket aromatic residues and the benzene lattice, were performed using the

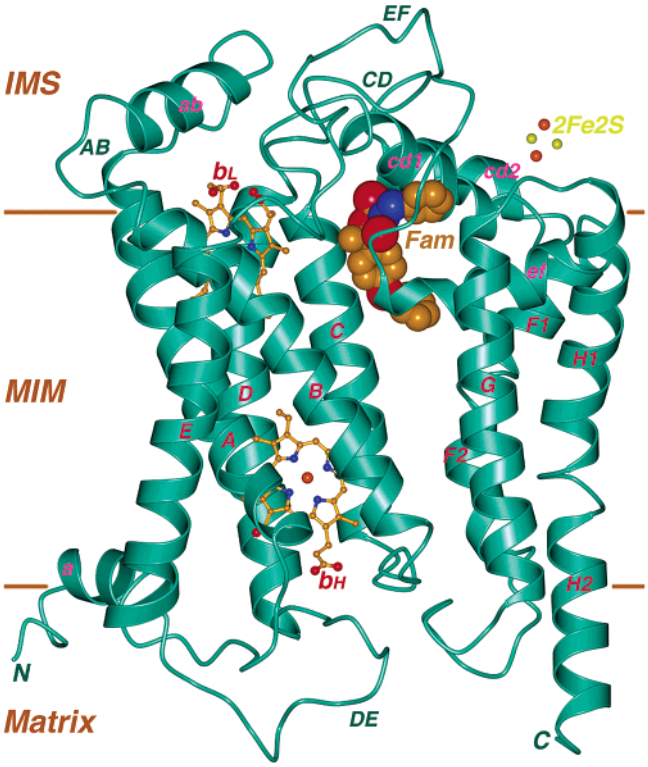

FIGURE 2: Ribbon representation of the cyt. *b* subunit structure with bound famoxadone. The eight TM helices are as labeled. The two intercalated hemes (b_L and b_H) are rendered as the ball-and-stick model. The bound famoxadone (Fam) is shown as the space-filling model with carbon atoms in yellow, oxygen in red, and nitrogen in blue. The 2Fe−2S cluster from subunit ISP is shown as balls with sulfur in yellow and iron in orange. Four prominent surface loops AB, CD, DE, and EF are as labeled. Within the surface loops, the helices are labeled as ab, cd1, cd2, and ef. The molecule is orientated similarly as in Figure 1 and the membrane bilayer is roughly delineated with the two parallel lines in brown.

least-squares option in O. Anomalous difference FFT calculations for the native and complex crystal were carried out using respective F^+-F^- as Fourier coefficients and separately refined model phases 90° rotated. Main chain and side chain conformation analyses between native and complex structure were performed with locally written programs (unpublished results).

RESULTS AND DISCUSSION

Structure of Cytochrome b with Bound Famoxadone. The *bc1* complex forms a dimer in solution. In the crystal of space group $I4_122$, each asymmetric unit contains a single *bc1* monomer consisting of 11 different subunits with 2,113 amino acid residues, three heme groups, and one *2*Fe−2S cluster (Figure 1). The refined native *bc1* has the crystallographic R_{free} and R_{work} of 29.7% and 26.1%, respectively (Table 1). We cocrystallized bovine *bc1* with the fungicide famoxadone. The inhibitor bound *bc1* protein behaved similarly to native protein in crystallization, but the cocrystals yielded better quality X-ray diffraction data sets (Table 1). The refined complex structure of *bc1* has the R_{free} and R_{work} of 30.6% and 25.9%, respectively, to 2.4 Å resolution. Figure 2 shows the structure of the cyt. *b* subunit in ribbon presentation with bound famoxadone in the refined *bc1* structure. The subunit has eight TM helices, labeled sequentially from A to H, arranged in two helical bundles: bundle I consists of helices A−E that incorporates two *b*-type hemes (b_L and b_H); bundle II is made of helices F−H. The two helical bundles contact each other at the matrix side of the membrane but separate from each other at the IMS, thus creating the so-called Q_o pocket between the two bundles near the IMS side, where the inhibitor famoxadone is located. The CD loop contains two helices cd1 and cd2 of 15 and 9 residues, respectively, arranged in a hairpin, providing a "lid" for the Q_o site and contributing residues to the docking site (the ISP crater) for interaction with ISP. The EF loop bridges between the two helical bundles as well as takes part in the formation of the ISP interaction site. Toward the end of the EF loop, there is a 12-residue helix, named ef, situated in a central position inside the Q_o pocket. The PEWY motif (270−273 in bovine), conserved in all organisms, is found at the beginning of the ef helix.

Conformational Flexibility and Binding Environment of Famoxadone. A difference Fourier synthesis between the famoxadone bound and native *bc1* crystal revealed a large piece of unassigned electron density in the Q_o pocket whose shape and size resembled that of famoxadone (Figures 3 and 4). The atomic model of famoxadone in the complex was built with the phenylamino group positioned near the binding crater of ISP directly underneath Y278 that is within H-bonding distance to H161, one of the ligands to 2Fe−2S cluster in ISP, while the phenoxyphenyl group remains at the entrance of the Q_o pocket (Figures 3 and 6a). In the complex, the famoxadone molecule displays a U shape with the phenylamino group and the phenoxy moiety in *syn* position, exhibiting a markedly different conformation from that observed in its crystalline state where famoxadone is in an extended *anti* conformation (*28*). Famoxadone is highly flexible by virtue of five dihedral angles in tandem and lack of significant steric hindrance (*28*); indeed, van der Waals

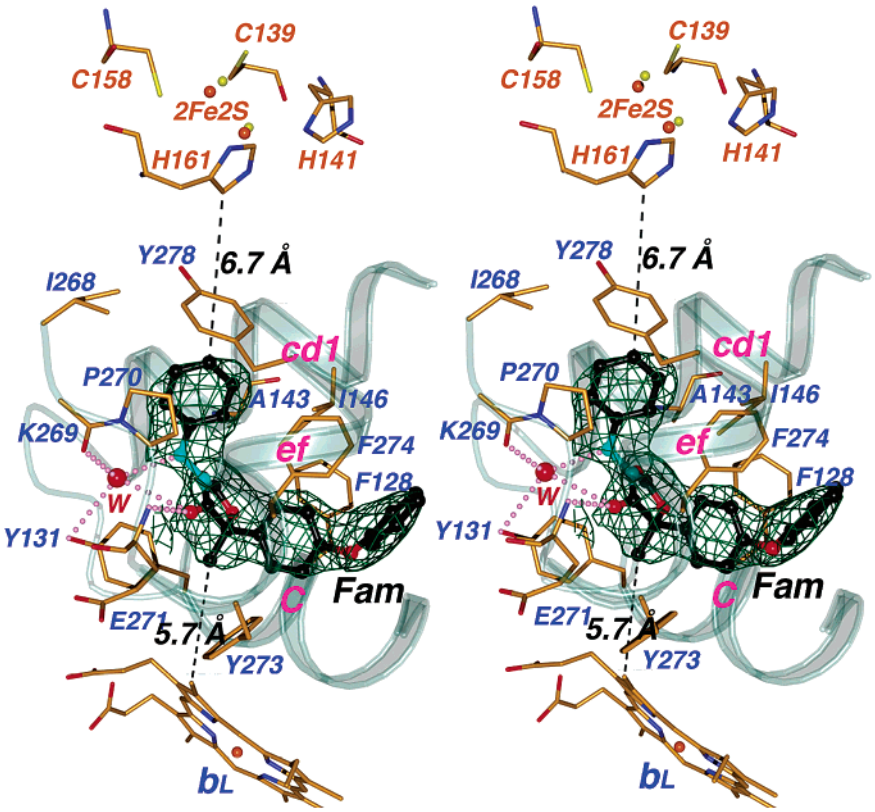

FIGURE 3: Stereopair of the famoxadone-binding environment in Q_o pocket. The famoxadone in the ball-and-stick model (Fam) is enclosed in the refined $2F_o-F_c$ electron density (dark green cage) contoured at 1.2 σ above mean. The nitrogen atoms for famoxadone are in light-green, oxygens in red, and carbons in black. The secondary structure elements that encompass the bound famoxadone in the Q_o pocket are from parts of helices C, cd1, and ef as shown. Residues interacting with famoxadone are drawn in the stick models and are as labeled. Hydrogen bonds are drawn in dotted lines; the water molecule that bridges the hydrogen bonding network is shown as a red ball and is labeled W. Four ligands to the 2Fe−2S from ISP subunit are shown as stick model. Distances from the bound famoxadone to the b_L heme and to the 2Fe−2S are drawn in black dashed lines.

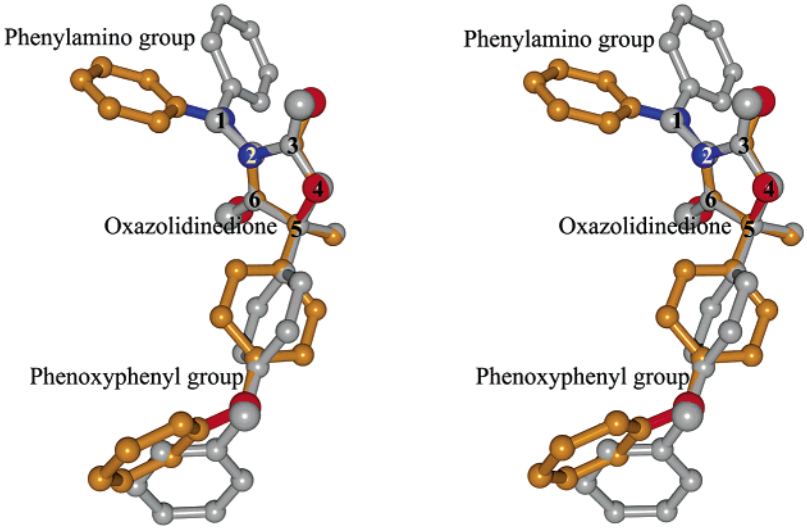

FIGURE 4: Stereopair of the structures of famoxadone in two different conformations. The three parts of the famoxadone are as labeled. The structure of free famoxadone from crystalline state is in gray, and that bound to the Q_o pocket of cyt. *b* is color-coded with carbon atoms in yellow, oxygen in red, and nitrogen in blue. The two structures are superimposed to each other on the five-member oxazolidinedione ring.

energies calculated for the *syn* and *anti* conformations are of −1.4 and −3.6 kcal/mol, respectively (*37*). The *anti* conformation in the crystalline state and the *syn* conformation in the complex are experimental manifestations of the conformational flexibility and adaptability of famoxadone to its environment.

Despite the H-bonding capabilities of the oxazolidinedione ring and the secondary amine group (N1), famoxadone prefers a hydrophobic and aromatic environment due to its three exposed phenyl groups. The portion of the Q_o pocket where famoxadone binds displays a "quarter-moon" shape, consisting of a front and a back part (Figure 6a). The front

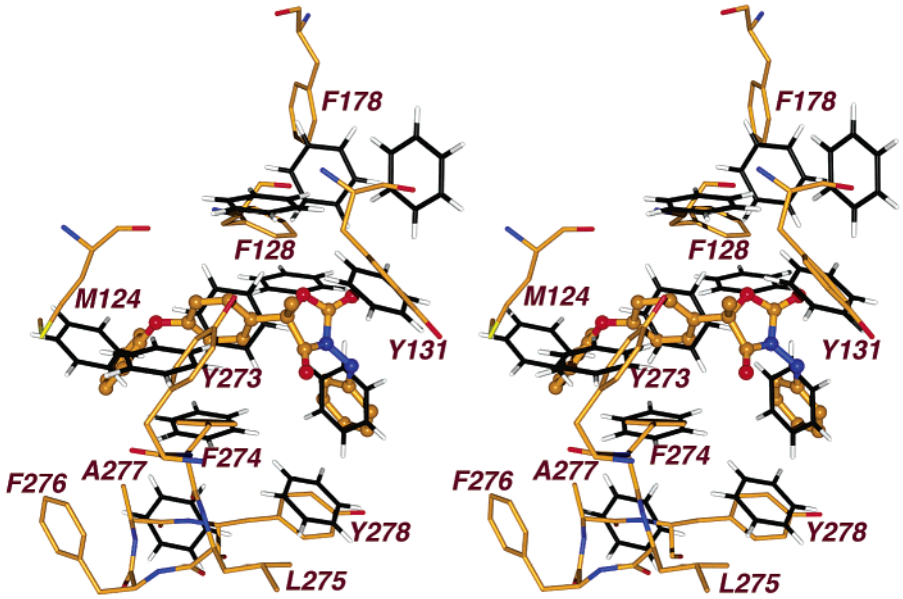

FIGURE 5: Stereopair showing specific Ar−Ar interactions between famoxadone and Q_o pocket residues. Superposition of a crystal lattice of benzene in the black-and-white stick model onto side chains of aromatic residues centered on the F274 within the Q_o pocket is demonstrated based on the result of least-squares method. The famoxadone and its protein environment are depicted as stick models with carbon atoms in yellow, oxygen in red, and nitrogen in blue.

entrance corridor consists of residues from helices C and F, the back ceiling is comprised of residues protruding from the cd1 and cd2 helix, and the back floor and wall are made up of residues from the ef helix (Figure 6a). Deep inside the Q_o pocket interacting with the phenylamino group of famoxadone are hydrophobic residues M138, G142, V145, I146, I268, P270, and Y278, of which V145, I268, and Y278 are part of the ISP docking crater (Figure 3). At the Q_o entrance, forming van der Waals interactions with the phenoxyphenyl group are hydrophobic residues M124, F128, I146, P270, Y273, F274, Y278, and I298. Among the three H-bonds formed between famoxadone and its protein environment, two are involved in an H-bonding network mediated through a structural water molecule (Figure 3): the N1 and O6 atom of famoxadone are 2.7 and 3.4 Å from the water molecule, respectively; on the protein side, the water molecule is held in place by two H-bonds to the carbonyl oxygen of K269 and the hydroxyl group of Y131 with distances of 2.8 and 3.7 Å, respectively. Another H-bond is formed between the carbonyl oxygen (O6) of famoxadone and the amide group of E271 with a distance of 2.5 Å. The closest distance of the famoxadone (C7) to the methyl group (CMD) of b_L heme is 5.7 Å, and that from the tip of phenylamino group to the CD2 of H161 of ISP, ligand to the 2Fe−2S cluster, is 6.7 Å (Figure 3). When a methyl group substitutes for the hydrogen atom at position N1 in the phenylamino group of famoxadone (Figure 4), the IC_{50} value for inhibition of mitochondrial ET increases by more than 3-fold, from 29 nM to 93 nM (*28*), demonstrating the importance of the water mediated H-bonding network, which is inevitably destroyed by the replacement of the hydrogen atom with a methyl group.

Significant Binding Affinity Is Derived from a Network of Ar−Ar Interactions. Although the elimination of the H-bonding network reduces *bc1* binding affinity for famoxadone by 3-fold, the methylated famoxadone remains tightly bound to the *bc1* complex with an IC_{50} of 93 nM as measured in rat submitochondrial particles (*28*). Therefore, there must be yet another source of significant interaction that contributes to the famoxadone binding affinity and that can only be derived from a network of Ar−Ar interactions. In the complex, the U-shaped famoxadone molecule with three aromatic rings is ideally suited for maximizing interactions with the aromatic ring of F274 (Figures 3 and 5). Least-squares superposition carried out on a part of crystal lattice of benzene type I (*23*) and the famoxadone-binding pocket centered on the phenyl side chain of F274 shows that the three aromatic rings of famoxadone as well as side chains of several aromatic residues (Figure 5) in the Q_o pocket coincide well with the benzene lattice for a network of Ar−Ar interactions with good agreement (rmsd of 2.1 Å for 10 pairs) and matching positions and orientations. In particular, famoxadone deploys all three of its aromatic rings to literally grasp the side chain of F274.

Both famoxadone and the aromatic residues lining the Q_o pocket have made significant conformational adjustments to optimize the Ar−Ar interactions. The phenyl ring in the phenoxyphenyl group and the terminal phenylamino group have rotated by nearly 90° and 180°, respectively, from their most stable conformation in the crystalline state (Figure 4), enabling them to form the Ar−Ar interactions with the phenyl group of F274, whose side chain swings nearly 6 Å from the native conformation (Table 2, Figure 6a). The fact that the terminal phenoxy ring in the phenoxyphenyl group is nearly perpendicular to its expected orientation in the benzene crystal lattice does not reduce its contribution to the binding, as here only short range and asymmetrical interactions are considered in the Q_o pocket. Additionally, F128, Y273, Y131, and F278 form four aromatic pairs with the bound famoxadone.

The network of Ar−Ar interactions expand beyond the first layer, involving next layer aromatic residues such as F178 forming a pair with F128 (Figure 5). These observations suggest that the very same force, which allows the crystallization of the macroscopically nonpolar benzene molecules at a temperature as high as +5.5 °C and presumably stabilizes

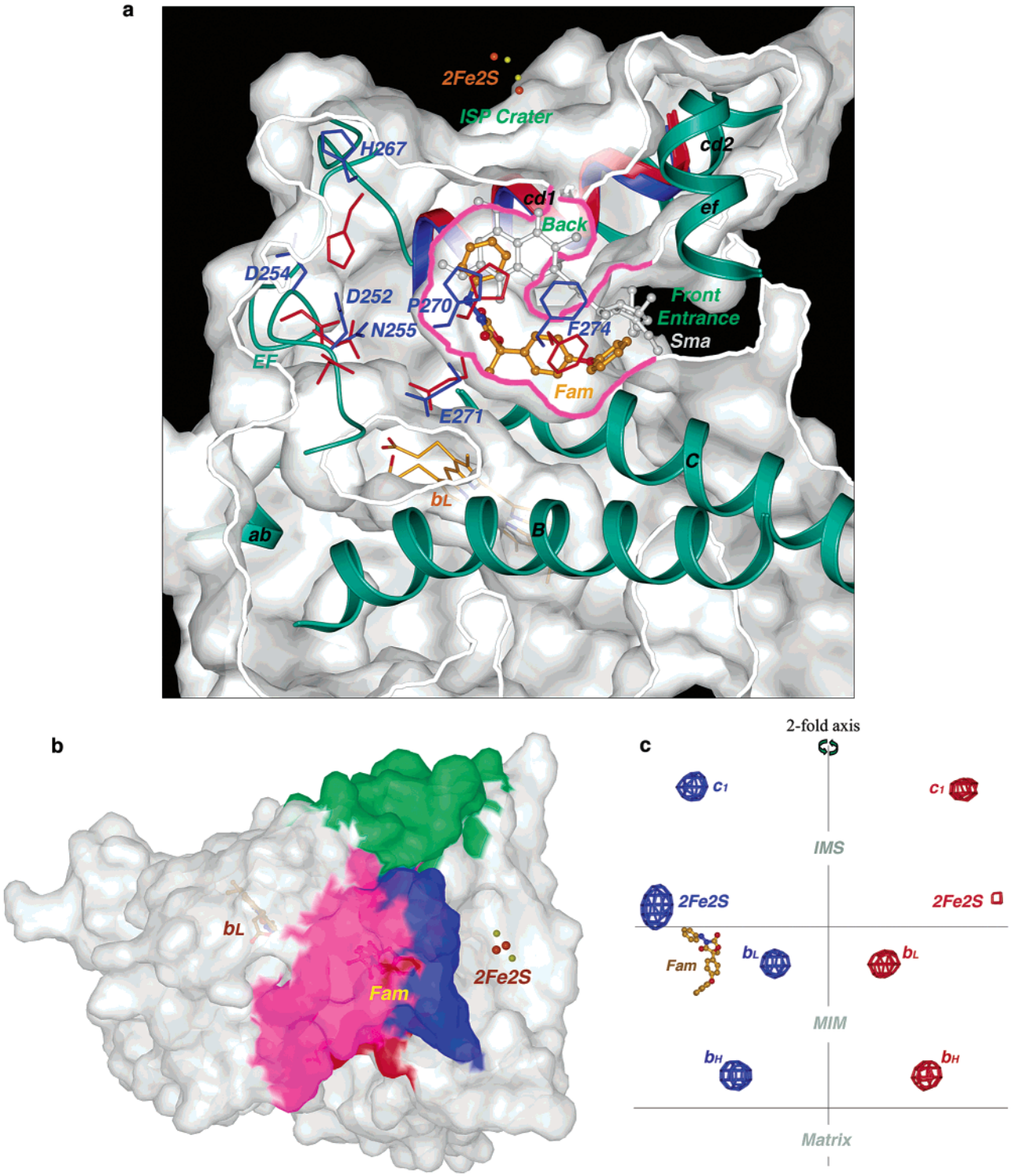

FIGURE 6: Conformational changes in *bc1* complex induced by famoxadone binding. (a) Cross-section of the cyt. *b* molecular surface in the vicinity of the Q_o pocket. The surface centered on the Q_o pocket is dissected with a vertical plane, and the border of the cutaway surface is outlined in white except for that lining the Q_o pocket which is colored magenta. Secondary structure elements and the b_L heme surrounding the Q_o site are shown. The famoxadone (Fam) is shown sitting in the quarter-moon-shaped Q_o pocket as the ball-and-stick model with the nitrogen atoms in blue, oxygen in red, and carbon in yellow. The front entrance and the back of the Q_o pocket are as labeled. Overlaid onto the Q_o pocket is the stigmatellin model (Sma) in gray found in the yeast structure for comparison (PDB code 1EZV). The residues undergoing large conformational changes are shown as stick model with native in red and famoxadone bound in blue. The cd1 helix in the inhibitor bound complex displaced downward by nearly 1 Å is shown as blue ribbon. The 2Fe−2S cluster of ISP is located above the Q_o pocket in a surface depression named the ISP crater. (b) Possible signal transduction pathway on the surface of cyt. *b*. Residues in cyt. *b*, which undergo large conformational changes both in main chain and side chain, are mapped onto the molecular surface. The surface patches are color-coded with type I residues in red, those contacting ISP neck region in green, those in ISP crater in blue, and the connecting patch in magenta. The surface is viewed roughly down the membrane normal from the IMS side. (c) Anomalous difference Fourier maps contoured at 5σ above mean for the irons in the *bc1* complex crystals with and without famoxadone. The right half in red shows the native anomalous difference Fourier, and the left half in blue gives the famoxadone bound form with the bound famoxadone as the ball-and-stick model. The two horizontal lines roughly indicate the mitochondrial inner membrane boundary. The vertical line marks the 2-fold molecular axis.

Table 2: Largest Changes in Distance between the Same Atoms of Equivalent Residues that Undergo Conformational Changes in the Presence and Absence of Famoxadone

type	residue name	atom type	distance (Å)	atom type	distance (Å)	environment
I[a]	I146	CA	0.9	CG1	1.4	In contact with the phenylamino group of famoxadone.
	K269	CA	2.3	NZ	2.3	
	P270	CA	1.9	CG	2.7	
	E271	CA	1.1	O	4.3	
	F274	CA	0.7	CE2	5.8	
II[b]	W163	CA	0.5	CH2	5.4	In contact with the ISP neck region.
	G166	CA	2.6	–	–	
	G167	CA	2.8	–	–	
	F168	CA	2.1	CZ	5.5	
	D171	CA	2.8	OD2	3.7	
	D252	CA	3.3	OD2	7.0	In the middle of EF loop.
	P253	CA	3.0	CG	4.0	
	D254	CA	2.9	OD2	7.2	
	N255	CA	1.5	ND2	2.5	
	Y256	CA	0.5	CE2	1.4	
	N263	CA	0.7	OD1	4.4	In the EF loop and part of ISP binding crater.
	T264	CA	0.4	OG1	1.9	
	P266	CA	0.9	CG	1.8	
	H267	CA	1.4	CE1	9.3	
	I268	CA	1.4	CD1	3.1	

[a] Residues that are in direct contact with famoxadone. [b] Residues that are not in direct contact with famoxadone but undergo induced conformational changes.

protein interior, is being employed by famoxadone to bind with high affinity to the Q_o pocket. The free energy contribution to the inhibitor binding from seven aromatic pairs is estimated to be between 7 and 14 kcal/mol, which is equivalent to that of three H-bonds (*25*, *26*). Mutations in cyt. *b* isolated from *S. cerevisiae* that greatly alter the binding capability of famoxadone are mostly substitutions of aromatic residues for aliphatic ones or vice versa in the Q_o pocket and provide strong support for the importance of Ar−Ar interaction in famoxadone binding (*27*). Two mutations produce particularly strong effects on the IC_{50} values: the F129L mutant (F128 in bovine) produces a 13-fold increase in the IC_{50} (120 vs 1569 nM) by disrupting interaction with the phenyl ring of the phenoxyphenyl group, whereas the L275F mutation (F274 in bovine) causes a 20-fold reduction in the IC_{50} (120 vs 5.8 nM) by gaining three Ar−Ar interactions and thus profoundly enhances the famoxadone binding affinity. Compared to the 3-fold increase in IC_{50} upon eliminating the H-bonding network, the network of Ar−Ar interactions should be regarded as a dominant force in famoxadone binding. This structural knowledge immediately suggests ways to improve the binding affinity of famoxadone and, more generally, provides a guideline for achieving high affinity ligand-protein interaction in a hydrophobic environment. It might be argued that the marked difference in binding affinity as a result of the two mutations, F129L and L275F, could be due to significant structural distortion on the part of cyt. *b* that either enhance or reduce famoxadone-binding ability. This interpretation is not favored since side chains of both residues are exposed to the cavity, and therefore would not produce significant structural alterations if changed. Indeed, F274 in bovine cyt. *b* is a natural variant of L275 in yeast (*S. cerevisiae*), and both enzymes are functional.

Famoxodone Binding Induced Conformational Changes. Structural changes in the cyt. *b* subunit due to binding of famoxadone are observed in the immediate environment of the inhibitor binding pocket and most noticeably in regions that make contacts with the ISP. The overall rmsd for C_α and for side chain atoms between the superimposed native and famoxadone bound cyt. *b* subunits are 0.5 and 1.0 Å, respectively, reflecting its overall structural rigidity. Using the criterion of 5 times rmsd that measures differences in main chain distances and side chain dihedral angles ($\chi1$ and $\chi2$) between equivalent residues, it can be shown that large structural motions in cyt. *b* involve residues centered around those listed in Table 2. For convenience, we refer to those residues involving in direct contact with and partially displaced by the bound famoxadone as type I. Five of them are given in Table 1: K269, P270, E271, and F274 near the PEWY sequence and I146 in the cd1 helix (Figures 3 and 6a). Type II residues are not in direct contact with famoxadone but undergo conformational changes in response to the inhibitor binding; they are found concentrated at the end of the CD loop and the proline-rich EF loop between helices E and ef (Figure 7, Table 2). Surprisingly the largest observed positional and dihedral movements involve residues in this category, which are distributed in a narrow strip on the surface of cyt. *b* from the inhibitor binding site to the binding surface for ISP (Figure 6b). The cd1 helix, as part of the ISP binding crater, moved nearly 1 Å downward in the inhibitor complex (Figure 6a), and the F helix shifted slightly in the lateral direction, opening up the Q_o pocket for famoxadone binding.

Cyt. *b* is considered a key player in the function of *bc1*, coordinating actions of various components of *bc1* in a catalytic cycle. One example that demonstrates the central role of cyt. *b* is the inhibitor binding at Q_o site induced large conformational changes in the ISP soluble domain (*13*). Type I residues may serve to adjust the size and shape of the Q_o pocket in order to accommodate the incoming inhibitor and to sense the presence or absence of inhibitor/substrate, whereas the type II residues relay and/or amplify conformational changes of type I residues at certain specific sites.

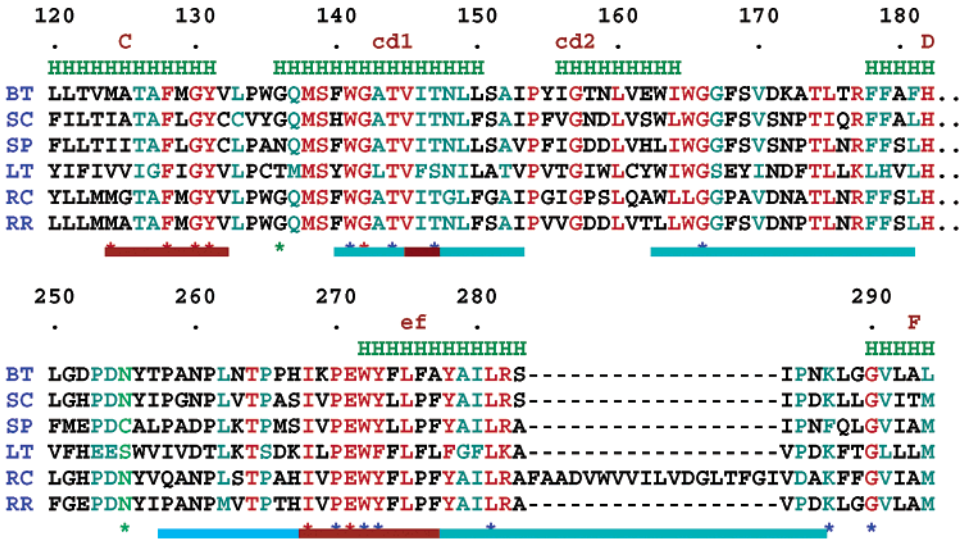

FIGURE 7: Sequence alignment of Q_o site residues. The Q_o site residues are composed of two segments: 120−182 and 250−294 in bovine sequence. Sequences include BT (*B. taurus*), SC (*S. cerevisiae*), SP (*S. pombe*), LT(*L. tarentolae*), RC (*R. capsulatus*), and RR (*R. rubrum*). The helical elements are indicated as consecutive Hs in green and are as labeled. Highly conserved residues (*44*) are colored red; moderately conserved residues are colored blue. Mutations of those residues that are labeled with red * inactivate quinol oxidation (*40*); those with blue * reduce quinol oxidation, and that with green * affect ISP assembly. Brown bars underneath the sequence indicate residues interacting with bound famoxadone; blue bars indicate interaction with ISP.

In this case, the type II residues are concentrated at three areas on the surface of the cyt. *b* subunit: the docking crater for the ISP soluble domain, the contact surface for the neck region of ISP, and the region that connects Q_o site to these two regions (Table 2, Figure 6b). It can therefore be speculated in the context of *bc1* function that the structural motif near the PEWY sequence would serve as a switch undergoing a bimodal motion in a *bc1* catalytic cycle, which is then relayed to the ISP crater and the neck contacting region via the ef loop to either capture or release ISP.

The most dramatic long-range conformational change is the switch of ISP from the loose state in the native crystal to the fixed state in the complex, as evidenced in the anomalous difference Fourier calculations for the native and famoxadone bound *bc1* crystal (Figure 6c). The b_L heme iron in the native crystal and that in the complex have anomalous peak heights of 0.97 and 0.99, respectively, after normalization to their respective b_H heme irons, suggesting a negligible change to these two heme groups. In contrast, the normalized anomalous peak heights in the complex for the cyt. *c1* iron is 0.775, up 41% from 0.551 in the native; that for the 2Fe−2S of ISP is 1.05, up 335% from 0.242 in the native. In fact, the anomalous peak for the 2Fe−2S cluster in native crystal is at noise level. These data demonstrate that binding of inhibitor stabilizes both cyt. *c1* and ISP and strongly favor ISP in the fixed conformation. The normalized peak height of 1.05 for the 2Fe−2S cluster anomalous signal (Figure 6c) suggests that ISP becomes less mobile upon binding of famoxadone and places this inhibitor in the same league as stigmatellin and UHDBT (*13*). A redox titration experiment in the presence of famoxadone showed a slight elevation (26 mV) in the midpoint potential from native for the ISP (unpublished results), whereas stigmatellin increases the ISP midpoint potential by as much as 250 mV. It is therefore experimentally evident that redox potential change in ISP is not linearly correlated to its mobility or position, a result inconsistent with the notion that midpoint potential reflects ISP equilibrium position in the Q_o site (*38*).

The famoxadone bound *bc1* effectively produced better quality crystals by reducing the cyt. *c1* and the ISP mobility, hence allowing better crystal packing. However, even with the reduced cell dimension by as much as 5 Å along the *c*-axis in the inhibitor bound *bc1* crystal (Table 1), the ISP subunit does not have significant lattice contact with neighboring *bc1* molecules. Improved crystal packing as a result of inhibitor binding may attribute partially to the pronounced enhancement of anomalous signals for the ISP iron in the complex crystal; the reduced mobility of ISP has to be a result of inhibitor binding because the anomalous peak height of cyt. *c1* does not increase nearly as much even though it is located in a similar crystal packing environment to the ISP.

Mechanism of Respiratory Inhibition. QH_2 oxidation at the Q_o site is initiated with the removal of the first proton followed by transfer of the first electron to the ISP and the second electron to the b_L heme. The binding of QH_2 or QH radical intermediate may involve hydrogen bonding of the hydroxyl groups with H161 (H181 in yeast) of the ISP subunit and E271 (E272 in yeast) of the cyt. *b* subunit, as implicated in the complex structure of yeast cyt. *b* with bound stigmatellin (*31*). Although structure overlay of the cyt. *b* subunit from yeast with bound stigmatellin to that from bovine with bound famoxadone produces an rmsd of only 0.7 Å, the difference in binding environment for stigmatellin and famoxadone is obvious. First, the headgroup of stigmatellin is 2.7 Å from H161 of ISP, whereas the closest distance between ISP and famoxadone is 6.7 Å (Figures 3 and 6a). Second, the side chain dihedral angle ($\chi 2$) of E271 in bovine is 150° away from that in yeast, where it is engaged in a critical hydrogen bond with stigmatellin. Third, the conformation of the phenyl group of F274 in bovine (L275 in yeast) would have interfered with stigmatellin binding. Recent structural and genetic experiments suggested the requirement of domain movement in ISP as part of the electron bifurcation mechanism of *bc1* function. Thus, the mechanism of ET inhibition by famoxadone appears 2-fold. One could be a

simple competition of inhibitor for the substrate binding site (*39*), assuming that famoxadone has far better binding affinity for the Q_o pocket than that of QH_2 molecule. The fact that the QH_2 molecule at Q_o site remains elusive crystallographically seems to confirm its lower binding affinity. The binding of famoxadone would stop QH_2 from getting close to the conserved PEWY motif, and the carboxylate group of E271 would not be available for hydrogen bonding. Mutations in residues that are in direct contact with famoxdone (Figure 7) result in reduced activity or defective in QH_2 oxidation (*40*), suggesting overlapping binding sites between QH_2 and famoxadone. On the other hand, the incomparable chemical structures of the inhibitor and substrate and the lack of competitive inhibition kinetics undermine this explanation. It is possible that the "true" quinol binding site may partially overlap or is nonsuperimposable with the inhibitor binding site; thus, binding of inhibitor does not interfere with substrate binding, although such an argument is not favored by the recent experiment with solid-state NMR technique to measure the ^{13}C-labeled quinol signal that is sensitive to Q_o site inhibitors (*39*). Furthermore, it has become evident that the proper function of *bc1* may require quinol to interact at multiple sites within the Q_o pocket, and hence the quinol motion, which is supported by the large available space within the Q_o pocket and the observation of multiple inhibitor binding sites (*6*, *11*, *13*−*15*). The second aspect of the possible inhibition mechanism is to stop the electron bifurcation at the Q_o site. The observation of a much enhanced anomalous signal for the 2Fe−2S cluster of ISP in the inhibitor bound complex indicates that the movement of ISP is severely hampered, resulting in the blockage of electron flow from ISP to cyt. *c1*.

Possible Control Mechanism for ISP Soluble Domain Movement. As a delicate molecular circuit, *bc1* complex is capable of diverging electrons from a quinol molecule in different directions following the Q cycle mechanism and coupling ET to proton translocation across membrane. Although the Q cycle hypothesis provides an overall mechanistic picture of *bc1* function, the issues of electron bifurcation at the Q_o site and its relation to the ISP movement as well as the release and capture mechanics of the ISP soluble domain require further experimental investigations. Table 2 provides a partial list of residues that undergo significant conformational changes as a result of famoxadone binding. Type I residues serve to accommodate inhibitor binding in the Q_o pocket. Mapping of type II residues reveals a strip on the surface of the cyt. *b* subunit connecting three surface areas: one area between residues 160−175 forms a contacting surface with the neck region of ISP (Figure 6b, green); another area involves residues between 262 and 268 that are part of the ISP docking crater (Figure 6b, blue); and the third area in the middle of the EF loop connects the Q_o pocket to the above-mentioned two surface areas (Figure 6b, magenta). It appears that the ef loop plays a role in detecting conformational changes in the Q_o pocket due to binding of substrate or inhibitors and subsequently redirecting the binding signal to the ISP neck contact and docking sites. Mutations for type I residues invariably destroy or reduce the rate of quinol oxidation (Figure 7, Table 2). For type II residues, one mutation, G166S, in the ISP neck contact area also slows down quinol oxidation (*40*). Two other mutations in the area that connects the Q_o site to the ISP neck contact and crater, N256Y and N256I in yeast (N255 in bovine, Figure 6a), affect the stability of the 2Fe−2S cluster of ISP (*40*) (Table 2). One of the residues in contact with ISP at the ISP crater which undergoes very large side chain conformational change is the H267 (Figure 6a); it is not completely conserved in the sequence alignment (Figure 7); yet all substitutions at this position are capable of forming H-bonds. The type II residues identified here appear critical in controlling ISP behavior as supported from prior mutational studies; their conformational changes illustrate the importance in function of the cyt. *b* subunit as a major driving force in *bc1* catalytic cycle and suggest the surface conformational strip as a possible signal transduction pathway within the cyt. *b* subunit serving to amplify the inhibitor binding signal to the conformational switch of ISP. Although speculative in their function, the key residues identified in our experiments in cyt. *b* subunit which undergo major conformational changes upon famoxadone binding provide an opportunity for future genetic and mutational analyses.

ACKNOWLEDGMENT

The authors wish to thank Dr. Z. Dauter and K. R. Rajashankar of X9B beamline at NSLS, BNL, Drs. R. Henning and Z. Ren of BioCARS beamline, and Drs. S. Weigand and Z. Wawrzak of DND beamline at APS, ANL, for their assistance in data collection. We thank Dr. F. Guo of LCB, NCI, NIH, for his help with synchrotron data collection, Drs. D. B. Jordon, S. O. Pember and Y. J. Zheng of Dupont for providing famoxadone, its crystal coordinates, and insightful discussion, and Drs. M. M. Gottesman and X. H. Ji of NIH for reading the manuscript.

REFERENCES

1. Hatefi, Y., Haavik, A. G., and Griffiths, D. E. (1962) *J. Biol. Chem. 237*, 1681−1685.
2. Brandt, U., and Trumpower, B. (1994) *Crit. Rev. Biochem. Mol. Biol. 29*, 165−197.
3. Trumpower, B. L., and Gennis, R. B. (1994) *Annu. Rev. Biochem. 63*, 675−716.
4. Gennis, R. B., Barquera, B., Hacker, B., Van Doren, S. R., Arnaud, S., Crofts, A. R., Davidson, E., Gray, K. A., and Daldal, F. (2001) *J. Bioenerg. Biomembr. 25*, 195−209.
5. von Jagow, G., Schagger, H., Riccio, P., Klingenberg, M., and Kolb, H. J. (1977) *Biochim. Biophys. Acta 462*, 549−558.
6. Xia, D., Yu, C. A., Kim, H., Xia, J. Z., Kachurin, A. M., Zhang, L., Yu, L., and Deisenhofer, J. (1997) *Science 277*, 60−66.
7. Xiao, K., Chandrasekaran, A., Yu, L., and Yu, C. A. (2001) *J. Biol. Chem. 276*, 46125−46131.
8. Mitchell, P. (1976) *J. Theor. Biol. 62*, 327−367.
9. Trumpower, B. L. (1990) *J. Biol. Chem. 265*, 11409−11412.
10. Trumpower, B. L. (1981) *J. Bioenerg. Biomembr. 13*, 1−24.
11. Zhang, Z., Huang, L., Shulmeister, V. M., Chi, Y. I., Kim, K. K., Hung, L. W., Crofts, A. R., Berry, E. A., and Kim, S. H. (1998) *Nature 392*, 677−684.
12. Iwata, S., Lee, J. W., Okada, K., Lee, J. K., Iwata, M., Rasmussen, B., Link, T. A., Ramaswamy, S., and Jap, B. K. (1998) *Science 281*, 64−71.
13. Kim, H., Xia, D., Yu, C. A., Xia, J. Z., Kachurin, A. M., Zhang, L., Yu, L., and Deisenhofer, J. (1998) *Proc. Natl. Acad. Sci. U.S.A. 95*, 8026−8033.
14. Xia, D., Kim, H., Yu, C. A., Yu, L., Kachurin, A., Zhang, L., and Deisenhofer, J. (1998) *Biochem. Cell Biol. 76*, 673−679.
15. Hunte, C., Koepke, J., Lange, C., Rossmanith, T., and Michel, H. (2000) *Structure. 15*, 669−684.
16. Tian, H., Yu, L., Mather, M. W., and Yu, C. A. (1998) *J. Biol. Chem. 273*, 27953−27959.
17. Tian, H., White, S., Yu, L., and Yu, C. A. (1999) *J. Biol. Chem. 274*, 7146−7152.

18. Darrouzet, E., Valkova-Valchanova, M., and Daldal, F. (2000) *Biochemistry 39*, 15475−15483.
19. Darrouzet, E., Moser, C. C., Dutton, P. L., and Daldal, F. (2001) *Trends Biochem. Sci. 26*, 445−451.
20. Ghosh, M., Wang, Y., Ebert, C. E., Vadlamuri, S., and Beattie, D. S. (2001) *Biochemistry 16*, 327−335.
21. von Jagow, G., and Link, T. A. (1986) *Methods Enzymol. 126*, 253−271.
22. Brugna, M., Rodgers, S., Montoya, G., Kazmeier, M., Nitschke, W., and Sinning, I. (2000) *Proc. Natl. Acad. Sci. U.S.A. 97*, 2069−2074.
23. Bacon, G. E., Curry, N. A., and Wilson, S. A. (1964) *Proc. R. Soc. London, Ser. A 279*, 98−100.
24. Flick, E. W. (1998) *Industrial Solvents Handbook*, 5th ed., Noyes Data Corporation, Westwood, NJ.
25. Burley, S. K., and Petsko, G. A. (1985) *Science 293*, 1793−1800.
26. Serrano, L., Bycroft, M., and Fersht, A. R. (1991) *J. Mol. Biol. 218*, 465−475.
27. Jordan, D. B., Livingston, R. S., Bisaha, J. J., Duncan, K. E., Pember, S. O., Picollelli, M. A., Schwartz, R. S., Sternberg, J. A., and Tang, X. S. (1999) *Pesticide Sci. 55*, 105−118.
28. Zheng, Y. J., Shapiro, R., Marshall, W. J., and Jordan, D. B. (2000) *Bioorg. Med. Chem. Lett. 10*, 1059−1062.
29. Yu, C. A., and Yu, L. (1980) *Biochim. Biophys. Acta 591*, 409−420.
30. Yu, C. A., Xia, D., Kim, H., Deisenhofer, J., Zhang, L., Kachurin, A. M., and Yu, L. (1998) *Biochim. Biophys. Acta 1365*, 151−158.
31. Otwinowski, Z., and Minor, W. (1997) *Methods Enzymol. 276*, 307−326.
32. Wilson, A. J. C. (1942) *Nature 150*, 152.
33. Murshudov, G. N., Vagin, A. A., and Dodson, E. J. (1997) *Acta Crystallogr. D53*, 240−255.
34. Read, R. J. (1986) *Acta Crystallogr. A42*, 140−149.
35. Ten Eyck, L. F. (1985) *Methods Enzymol. 115*, 324−337.
36. Jones, T. A., Zou, J. Y., Cowan, S. W., and Kjeldgaard, M. (1991) *Acta Crystallogr. A47*, 110−119.
37. Dauber-Osguthorpe, P., Roberts, V. A., Osguthorpe, D. J., Wolff, J., Genest, M., and Hagler, A. T. (1988) *Proteins: Struct., Funct., Genet. 4*, 31−47.
38. Darrouzet, E., Valkova-Valchanova, M., and Daldal, F. (2002) *J. Biol. Chem. 277*, 3464−3470.
39. Bartoschek, S., Johansson, M., Geierstanger, B. H., Okun, J. G., Lancaster, C. R., Humpfer, E., Yu, L., Yu, C. A., Griesinger, C., and Brandt, U. (2001) *J. Biol. Chem. 276*, 35231−35234.
40. Brasseur, G., Saribas, A. S., and Daldal, F. (1996) *Biochim. Biophys. Acta 1275*, 61−69.
41. Nicholls, A., Sharp, K. A., and Honig, B. (1991) *Proteins: Struct., Funct., Genet. 11*, 281−296.
42. Kraulis, P. J. (1991) *J. Appl. Crystallogr. 24*, 946−950.
43. Esnouf, R. M. (1997) *J. Mol. Graph. 15*, 133−138.
44. Degli Esposti, M., De Vries, S., Crimi, M., Ghelli, A., Patarnello, T., and Meyer, A. (1993) *Biochim. Biophys. Acta 1143*, 243−271.

BI026252P